THE JOURNAL OF PHYSICAL CHEMISTRY C

Article

Cite This: J. Phys. Chem. C 2018, 122, 26570−26575

pubs.acs.org/JPCC

Enhanced Photocatalytic Activity of 2H-$MoSe_2$ by 3d Transition-Metal Doping

Yafei Zhao,[†] Jian Tu,[†] Yizhe Sun,[†] Xiaoying Hu,[‡] Jiai Ning,[†] Wei Wang,[†] Fengqiu Wang,[†] Yongbing Xu,[†] and Liang He*[,†]

[†]National Laboratory of Solid State Microstructures, School of Electronic Science and Engineering and Collaborative Innovation Center of Advanced Microstructures, Nanjing University, Nanjing 210093, China

[‡]College of Science and Laboratory of Materials Design and Quantum Simulation, Changchun University, Changchun 130022, China

Supporting Information

ABSTRACT: To develop $MoSe_2$-based photocatalysts, increasing the catalytic activity of 2H-$MoSe_2$ is essential. In this work, the electronic and photocatalytic properties of 3d transition metal-doped (Sc, Ti, V, Cr, Mn, Fe, Co, Ni, Cu, and Zn) 2H-$MoSe_2$ were investigated by first-principles calculations. The results indicate that Sc, Ti, V, Cr, Mn, Fe, and Co atoms tend to substitute the Mo atoms under a Se-rich condition, whereas Ni, Cu, and Zn atoms prefer to occupy the interstitial positions. More importantly, Sc- and Ti-doped 2H-$MoSe_2$ can enhance the photocatalytic activity by increasing the oxidizability of photogenerated holes, suppressing the recombination of photogenerated carriers, and increasing the number of catalytic active sites.

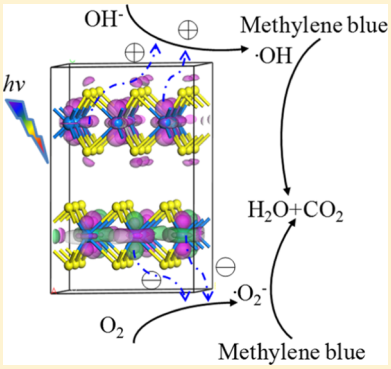

1. INTRODUCTION

As a member of the transition-metal dichalcogenide (TMDC) material, hexagonal $MoSe_2$ has three kinds of structures, such as 1T, 2H, and 3R phases, and the 2H phase is the most stable one.[1−3] Recently, 2H-$MoSe_2$ has stimulated considerable worldwide attention because of its potential catalytic applications in photocatalytic degradation of organic pollutants.[4−6] However, its active sites only exist at the edges states and the high recombination rate limits its applications as a photocatalyst.[7,8] Theoretical and experimental studies have shown that doping is a promising method to improve the photocatalytic activity of $MoSe_2$[9,10] because the impurity levels (ILs) generated by dopants can decrease the recombination rate of photogenerated carriers.[11−14] However, a systematic study of the effect of 3d TMs on catalytic active sites and oxygen reduction reaction (ORR) of 2H-$MoSe_2$ is needed.

In this work, using first-principles calculations, we have studied the electronic and photocatalytic properties of 3d TM-doped 2H-$MoSe_2$. It is found that Sc, Ti, V, Cr, Mn, Fe, and Co atoms tend to occupy the Mo site under the Se-rich condition, whereas Ni, Cu, and Zn atoms prefer to occupy the interstitial sites of B_{Se}, B_{Se}, and H, respectively. Moreover, Sc- and Ti-doped systems can further enhance the photocatalytic activity of 2H-$MoSe_2$ by separating the highest occupied molecular orbital (HOMO) and the lowest unoccupied molecular orbital (LOMO), suppressing the recombination of photogenerated electrons (e^-)/holes (h^+), increasing the number of active sites, and enhancing the oxidizability of photogenerated h^+.

2. COMPUTATIONAL DETAILS

A first-principles study was performed using the Vienna Ab-initio simulation package on the basis of the projected augmented wave potential approach.[15−17] The Perdew−Burke−Ernzerhof function of the generalized gradient approximation was used as the exchange correlation function.[18,19] To simulate the doping model of 3d TM atoms in a 3 × 3 × 1 supercell 2H-$MoSe_2$ with 18 Mo and 36 Se atoms, we considered the TM atoms substituting Mo atoms (TM_S) (Figure 1a,b) or occupying the interstitial position (TM_i); thus, the atomic doping ratio (TM/Mo) is 5.88 or 5.56%.

In addition, the TM_i-doped system has three doped cases: the position directly below the upper layer Mo atom (B_{Mo}); the position directly below the upper layer Se atom (B_{Se}); and the position above the hollow site (H) of the hexagonal rings of the lower layer (Figure 1a,c,d). In fact, B_{Mo} and B_{Se} describe the same position according to the symmetry of 2H-$MoSe_2$. Details on calculation parameters can be found elsewhere.[20] In addition, the total energy was corrected using Grimme's DFT-D2 method and is used to describe the VDW interactions.[21,22]

Received: September 25, 2018
Revised: October 30, 2018
Published: October 31, 2018

DOI: 10.1021/acs.jpcc.8b09361
J. Phys. Chem. C 2018, 122, 26570−26575

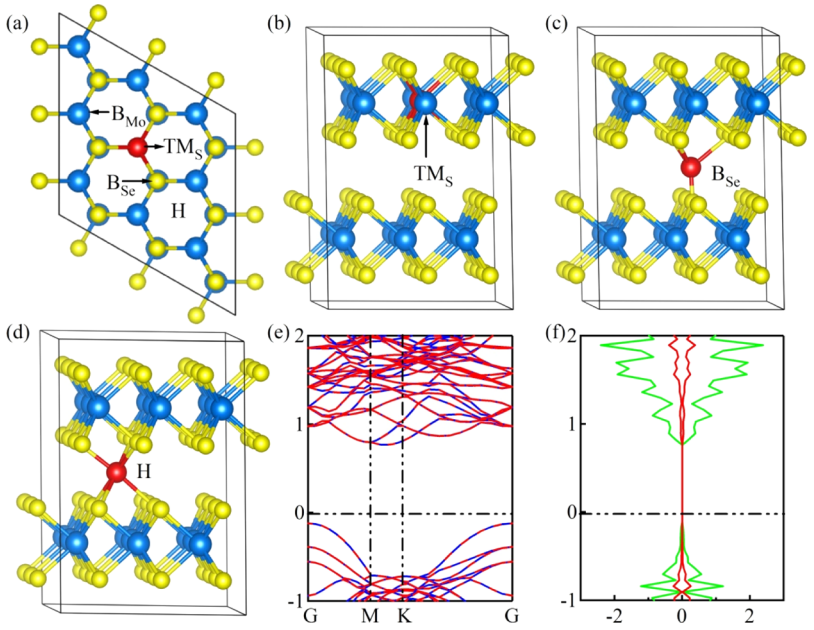

Figure 1. Three different interstitial sites and one substitute site of 2H-$MoSe_2$: top view (a) and side view (b–d). The blue, yellow, and red spheres denote Mo, Se, and TM atoms, respectively. The band structure (e) and average PDOS (f) of undoped 2H-$MoSe_2$.

We have calculated the formation energy (E_f) of all doped systems to assess the stability of different TM dopants

$$E_f = E_{doped} - E_{undoped} + m\mu_{Mo} - n\mu_{TM} \quad (1)$$

E_{doped} and $E_{undoped}$ are the total energies of 2H-$MoSe_2$ with and without a TM atom and μ_{TM} is the chemical potential of the per TM atom in bulk TM. The coefficients m and n represent the number of substituted Mo atoms and the number of TM atoms introduced into the supercell, respectively. E_f is changing from the Mo-rich condition to the Se-rich condition. Relations between μ_{Mo} and μ_{Se} are as follows

$$\mu_{Mo} + 2\mu_{Se} = \mu(MoSe_2) \quad (2)$$

Under the Se-rich condition, μ_{Se} is the chemical potential of the per Se atom in bulk Se, and μ_{Mo} is obtained from eq 2. Under the Mo-rich condition, μ_{Mo} is obtained from the energy of one Mo atom in bulk Mo, and μ_{Se} is determined by eq 2. Negative E_f suggests that TM atoms are very easy to enter the 2H-$MoSe_2$ lattice.

3. RESULTS AND DISCUSSION

3.1. Formation Energies and Optimized Structures. Figure 2 lists the E_f values of TM-doped 2H-$MoSe_2$. It is found that the E_f of the TM_S-doped system obtained under the Se-rich condition is smaller than that under the Mo-rich condition because more Mo vacancies are present in the Se-rich condition. E_f increases as the atomic number of the dopant atoms increases, except for the Cu-doped system. Second, the total energies of TM_i (B_{Se} or H)-doped systems were calculated and compared, and the results showed that Sc, Ti, and Zn atoms tend to occupy the H site and that V, Cr, Mn, Fe, Co, Ni, and Cu atoms prefer to occupy the B_{Se} site. The E_f of each most stable TM_i-doped system (E_i) is shown in Figure 2.

Moreover, by comparing the E_f of TM_S- and TM_i-doped systems, we found that Sc, Ti, V, Cr, Mn, Fe, and Co atoms tend to substitute the Mo atoms, whereas Ni, Cu, and Zn atoms prefer to occupy the positions of B_{Se}, B_{Se}, and H sites,

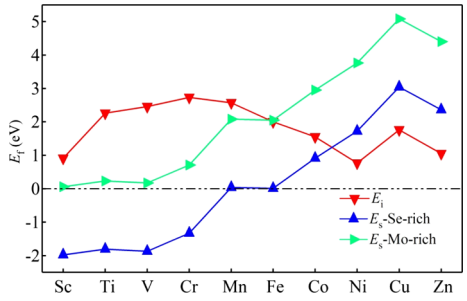

Figure 2. E_f of the TM-doped 2H-$MoSe_2$. The results indicate that Sc, Ti, V, Cr, Mn, Fe, and Co atoms prefer to substitute Mo atoms under the Se-rich condition, whereas Ni, Cu, and Zn atoms prefer to occupy the interstitial sites.

respectively. The reason is that the atomic radius of a Ni atom is the smallest among all 3d TM atoms, so it is easy to appear at the interstitial site. For Cu and Zn atoms, because their 3d orbitals are fully occupied, the ability to lose electrons is weak, and thus they are difficult to replace Mo atoms. Further, the results of the electronic density difference suggest that Ni_{Se} and Cu_{Se} are chemical adsorption, whereas Zn_H is physical adsorption (Figure S1, Supporting Information).

Overall, all doped systems can be realized by thermal dynamically preferred methods because they have a small E_f (−1.98 to 0.77 eV), except for Cu_{Se}- and Zn_H-doped systems. However, Cu_{Se}- and Zn_H-doped (1.76 and 1.05 eV) 2H-$MoSe_2$ can still be synthesized by nonequilibrium methods such as molecular beam epitaxy and post-synthesis techniques.[23−25]

3.2. Electronic Properties. 2H-$MoSe_2$ is an indirect band gap semiconductor with an indirect band gap of 0.89 eV,[26,27] and the conduction band (CB) and the valence band (VB) are composed of Mo 4d and Se 4p states, as shown in Figure 1e,f. Figure 3 only illustrates the band structure and the average partial density of states (PDOS) of Mo, Se, and TM atoms for each most stable TM-doped systems. It is found that the electronic properties of Cr-doped 2H-$MoSe_2$ are similar to those of undoped one because the Cr element also belongs to

DOI: 10.1021/acs.jpcc.8b09361
J. Phys. Chem. C 2018, 122, 26570−26575

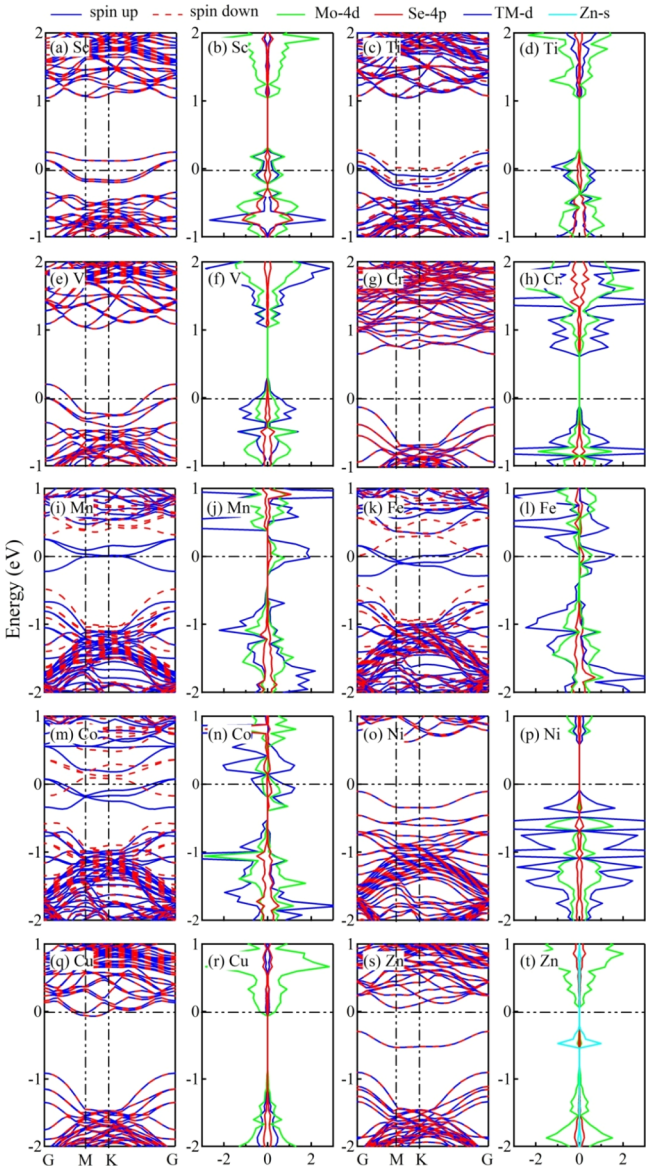

Figure 3. Band structure and average PDOS of TM-doped 2H-$MoSe_2$. Except for Cu-doped $MoSe_2$, the ILs are located within the band gap. The Sc-, Cr-, Mn-, Fe-, and Co-doped systems are direct band gap semiconductors.

the VIB group as Mo. Second, substitutional doping by Sc, Ti, and V atoms creates ILs (mostly composed of TM 3d and Mo 4d states) sitting within the VB maximum (VBM) and the Fermi levels move into the VB, resulting in the p-type conductivity and metallic properties, consistent with the reported results,[28,29] as shown in Figure 3a,c,e. This can be attributed to the fact that the acceptor dopants can easily introduce some holes into the 2H-$MoSe_2$ lattice.

In Mn-, Fe-, and Co-doped systems, the ILs (TM 3d and Mo 4d states) are close to or overlap with the CB minimum (CBM), and the Fermi levels cross the CBM (see Figure 3i,k,m). Thus, they become n-type semiconductors and exhibit metallic properties, as the substitutional donor TM atoms introduce additional electrons into the system. Similarly, Cu- and Zn-doped systems are also n-type semiconductors, but the Ni dopant only makes the Fermi level rise a small distance. Moreover, the ILs (Zn 4s states) are within the band gap of the Zn-doped system. However, there is no ILs in the band gap of the Cu-doped system because its d orbit is the full electron state. In addition, we have found that Sc-, Cr-, Mn-, Fe-, and Co-doped systems are direct semiconductors which can improve the absorption efficiency of light. This is essential for practical applications of optoelectronic devices.

In summary, we have already found that TM dopants can change the electronic structure, such as the number and shape of the ILs (flat or curvature), the energy position of the CBM (E_{CBM}) and VBM (E_{VBM}), and the composition of the CBM and VBM. Thus, they can modulate the photocatalytic activity.

In fact, when we discuss the photocatalytic ability of common semiconductors, there are four key concerns, such as suitable band gap value, low e^-/h^+ recombination rate, rich catalytic active site, and suitable work function for ORR.[30−32] 2H-$MoSe_2$-based catalysts have inherently excellent optical absorption properties (absorbing all visible light). Therefore, we only need to explore the other three factors, and more details will be discussed later.

3.3. Effective Mass of Photogenerated Carriers. The ILs within the band gap can facilitate photoexcited e^- pumping from the VB into the CB. It should be noted that curved and broad ILs can reduce the e^-/h^+ recombination, whereas the e^- trapped in the flat ILs is easily annihilated by recombination with h^+.[7,31] To quantify the recombination rate of ILs, the effective mass (m^*) has been calculated and is listed in Table 1. The smaller m^* suggests higher mobility ($\mu = e\tau/m^*$) and higher chances for the photogenerated carriers to get to the

Table 1. Summary of Calculated Results of TM-Doped $MoSe_2$[a]

system	Sc	Ti	V	Cr	undoped	Mn	Fe	Co	Ni	Cu	Zn
site	TM_s	TM_s	TM_s	TM_s		TM_s	TM_s	TM_s	B_{Se}	B_{Se}	H
E_{CBM}	5.83	5.89	5.88	5.77	5.91	5.80	5.72	5.53	5.89	5.86	5.84
E_{VBM}	4.91	4.96	4.89	4.99	5.02	4.89	4.95	4.78	4.85	5.01	4.88
E_g	0.92	0.93	0.99	0.78	0.89	0.91	0.77	0.75	1.03	0.85	0.96
m_e^*	0.90	0.91	0.92	1.06	0.99	1.04	1.07	1.02	1.01	1.04	1.25
m_{ILs}^*	1.33	1.39	1.01			1.46	1.34	1.76	1.67		1.04
		1.37				1.54	1.73	1.73			
		0.84				1.10	1.02	1.01			
						1.78	1.43	1.83			
m_h^*	1.29	1.28	1.23	1.37	1.26	1.35	1.32	1.35	1.33	1.36	1.46
R	1.43	1.41	1.34	1.29	1.27	1.30	1.23	1.32	1.32	1.31	1.17

[a]Site represents the doping position of various TM atoms. E_{CBM}, E_{VBM}, and E_g are the energy positions of CBM, VBM, and band gap in eV, respectively. m_e^*, m_{ILs}^*, and m_h^* are the effective mass of electrons, ILs, and holes in m_e, respectively. $R = m_h^*/m_e^*$ is the relative effective mass.

DOI: 10.1021/acs.jpcc.8b09361
J. Phys. Chem. C 2018, 122, 26570−26575

surface.[33−35] It is found that all doped systems have smaller m^* (0.84−1.83) of ILs (m^*_{ILs}); thus, they are curved and broad ILs and can reduce the recombination rate of e^-/h^+.

Moreover, the large difference between m^* of the e^- (m^*_e) and h^+ (m^*_h) results in the large difference of diffusion length (L_p), $L_p = \sqrt{\frac{\mu k_b T \tau}{e}} = \sqrt{\frac{k_b T \tau^2}{m^*}}$.[33,34] Thus, the relative mass ($R = m^*_h/m^*_e$) has been used to evaluate the recombination rate.[36] It is found that Sc- and Ti-doped 2H-$MoSe_2$ have the largest R, suggesting that they can greatly reduce the recombination of photogenerated carriers; see Table 1.

3.4. Photocatalytic Properties. Catalytic active sites were defined by the HOMO and LOMO. As shown in Figure 4a, the HOMO and LUMO of 2H-$MoSe_2$ are located at all Mo atoms simultaneously; thus, most of the photogenerated e^-/h^+ will be recombined on Mo atoms immediately.

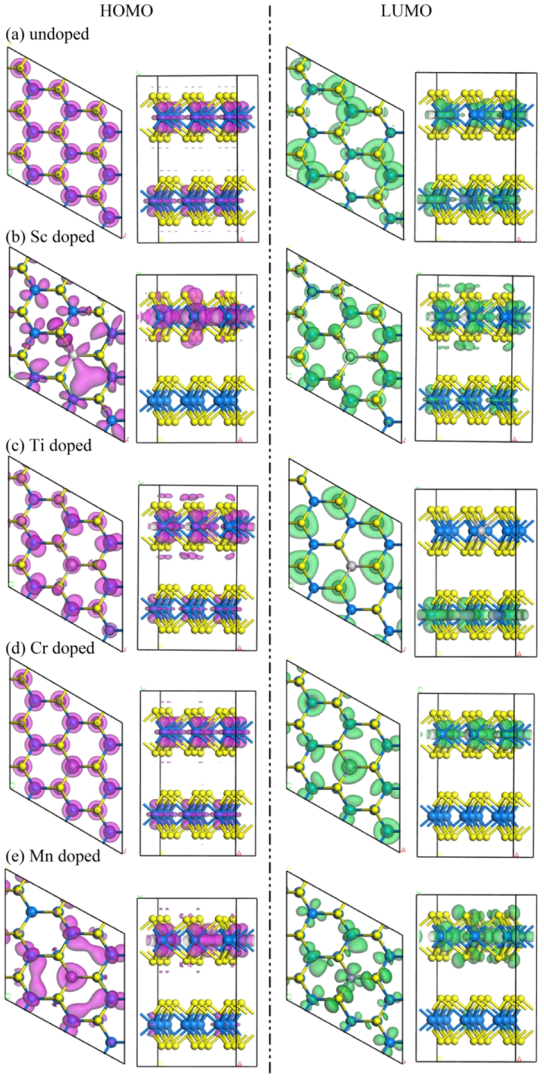

Figure 4. HOMO and LUMO of TM-doped and undoped 2H-$MoSe_2$. The isosurface is taken at a value of 0.03 e/bohr^3. The purple and green regions represent HOMO and LUMO, respectively. Ti-, Cr-, and Mn-doped systems are demonstrated as examples, and for other doped systems, please refer to Figure S2. The HOMO and LUMO of Sc-, Ti-, and Cr-doped 2H-$MoSe_2$ are separated in real space.

For Sc-doped 2H-$MoSe_2$, HOMO is located only on the Mo and Sc atoms of the upper layer, whereas LUMO is similar to 2H-$MoSe_2$ (Figure 4a,b). For Ti- and V- and Ni-, Cr-, Co-, and Cu-doped 2H-$MoSe_2$, the HOMO is similar to 2H-$MoSe_2$. In Ti-, V-, and Ni-doped systems, the LUMO is located only on Mo atoms in the lower layer (Figure 4c is the case of a Ti-doped system. For other doped systems, please refer to Figure S2a,d). However, the LUMO in Cr-, Co-, and Cu-doped systems is located on Mo atoms in the upper layer (Figure 4d is the case of a Cr-doped system. For other doped systems, please refer to Figure S2c,e, Supporting Information). The reason is that the composition of VBM and CBM has been changed by the dopant, as shown in Figure 3. Overall, in these seven cases, the HOMO and LUMO are separated, and the number of catalytic active sites is increased dramatically. However, the HOMO and LUMO states of Mn- and Fe-doped systems are mostly located on the Mo and TM atoms of the upper layer (Figure 4e is the case of a Mn-doped system. For other doped systems, please refer to Figure S2b, Supporting Information). For Zn-doped 2H-$MoSe_2$, the HOMO and LUMO are similar to 2H-$MoSe_2$ (Figure S2f, Supporting Information). Thus, the photogenerated e^-/h^+ has a good chance to recombine in those systems.

Further, Figure 5 illustrates the mechanism of photocatalytic degradation of methylene blue by using Ti-doped 2H-$MoSe_2$

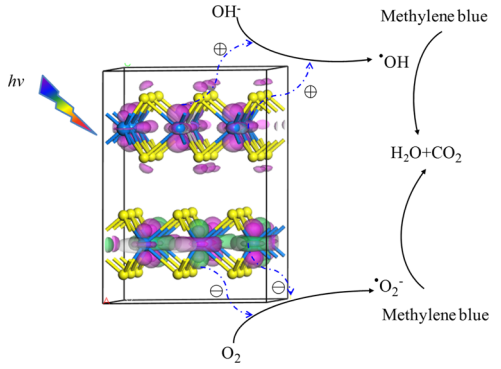

Figure 5. Mechanism of photocatalytic degradation of an organic pollutant and the charge dynamics in Ti-doped 2H-$MoSe_2$. Under light irradiation, the photogenerated electrons move to the Mo atoms in the green region (LUMO), whereas photogenerated holes move to the Mo and Ti atoms in the purple region (HOMO). This represents the separation of photogenerated e^-/h^+ in real space.

as an example. Under light irradiation, e^- and h^+ will be generated at the green and purple regions, respectively. O_2^- ions (or $^\bullet$OH radicals) can be reduced (or oxidized) by e^- (or h^+). Then, methylene blue can be oxidized to H_2O and CO_2. Thus, the amount of e^- or h^+ that reaches the surface of the catalyst determines the photocatalytic activity of the catalyst. The Ti dopant can greatly improve the photocatalytic performance of 2H-$MoSe_2$ because it can reduce the recombination rate of carriers and increase the number of photocatalytic active sites. This effect is similar to the results of previous theoretical and experimental reports.[6,12,30,37]

On the other hand, E_{CBM} and E_{VBM} of undoped and TM-doped 2H-$MoSe_2$ are calculated relative to the vacuum level.[38] We have found that E_{VBM} and E_{CBM} of all doped systems move down to the low-energy region compared with those of undoped 2H-$MoSe_2$. Therefore, the oxidizability of photogenerated h^+ at the HOMO is enhanced, whereas the

DOI: 10.1021/acs.jpcc.8b09361
J. Phys. Chem. C 2018, 122, 26570−26575

reducibility of photogenerated e^- at LUMO is reduced. This suggests that a $^{\bullet}OH$ radical plays a leading role in the photocatalytic degradation process.

4. CONCLUSIONS

In this work, doping site, formation energy, and electronic and photocatalytic properties of 3d-TM-doped 2H-$MoSe_2$ were investigated by first-principles calculations. The results indicate that the Se-rich condition is energetically favorable to substitute Mo atoms by Sc, Ti, V, Cr, Mn, Fe, and Co atoms, whereas the Ni, Cu, and Zn atoms preferentially occupy the interstitial position. Moreover, Sc- and Ti-doped 2H-$MoSe_2$ have demonstrated excellent photocatalytic activity because they can suppress the recombination of photogenerated e^-/h^+, separate HOMO and LUMO, enhance oxidizability of photogenerated h^+, and increase the number of photocatalytic active sites. This work provides an important guidance for developing 2H-$MoSe_2$-based photocatalysts.

■ ASSOCIATED CONTENT

Supporting Information

The Supporting Information is available free of charge on the ACS Publications website at DOI: 10.1021/acs.jpcc.8b09361.

Electron density difference of TM-doped 2H-$MoSe_2$ and HOMO and LUMO of TM-doped 2H-$MoSe_2$ (PDF)

■ AUTHOR INFORMATION

Corresponding Author

*E-mail: heliang@nju.edu.cn.

ORCID

Fengqiu Wang: 0000-0001-9823-5788

Liang He: 0000-0002-5279-0097

Notes

The authors declare no competing financial interest.

■ ACKNOWLEDGMENTS

This work is supported by the National Key Research and Development Program of China (no. 2016YFA0300803, 2017YFA0206304) and the National Natural Science Foundation of China (no. 61474061, 61674079). Jiangsu Shuangchuang Program and the Natural Science Foundation of Jiangsu Province of China (no. BK20140054).

■ REFERENCES

(1) Yu, Y.; Nam, G.-H.; He, Q.; Wu, X.-J.; Zhang, K.; Yang, Z.; Chen, J.; Ma, Q.; Zhao, M.; Liu, Z.; et al. High phase-purity 1T′-MoS_2- and 1T′-$MoSe_2$-layered crystals. *Nat. Chem.* **2018**, *10*, 638−643.

(2) Ambrosi, A.; Sofer, Z.; Pumera, M. 2H → 1T phase transition and hydrogen evolution activity of MoS_2, $MoSe_2$, WS_2 and WSe_2 strongly depends on the MX_2 composition. *Chem. Commun.* **2015**, *51*, 8450−8453.

(3) Lee, J.; Kang, S.; Yim, K.; Kim, K. Y.; Jang, H. W.; Kang, Y.; Han, S. Hydrogen Evolution Reaction at Anion Vacancy of Two-Dimensional Transition-Metal Dichalcogenides: Ab Initio Computational Screening. *J. Phys. Chem. Lett.* **2018**, *9*, 2049−2055.

(4) Tian, T.; Rice, P.; Santos, E. J. G.; Shih, C.-J. Multiscale Analysis for Field-Effect Penetration Through Two-Dimensional Materials. *Nano Lett.* **2016**, *16*, 5044−5052.

(5) Yang, Y.; Wang, S.; Zhang, J.; Li, H.; Tang, Z.; Wang, X. Nanosheet-assembled $MoSe_2$ and S-doped $MoSe_{2-x}$ nanostructures for superior lithium storage properties and hydrogen evolution reactions. *Inorg. Chem. Front.* **2015**, *2*, 931−937.

(6) Zhao, Y.; Wang, W.; Li, C.; Sun, Y.; Xu, H.; Tu, J.; Ning, J.; Xu, Y.; He, L. Enhanced photocatalytic activity of nonmetal doped monolayer $MoSe_2$ by hydrogen passivation: First-principles study. *Appl. Surf. Sci.* **2018**, *456*, 133−139.

(7) Li, Z.; Meng, X.; Zhang, Z. Recent development on MoS_2 -based photocatalysis: A review. *J. Photochem. Photobiol., C* **2018**, *35*, 39−55.

(8) Kibsgaard, J.; Chen, Z.; Reinecke, B. N.; Jaramillo, T. F. Engineering the surface structure of MoS_2 to preferentially expose active edge sites for electrocatalysis. *Nat. Mater.* **2012**, *11*, 963−969.

(9) Zhao, Y. F.; Wang, W.; Li, C.; He, L. First-Principles Study of Nonmetal Doped Monolayer $MoSe_2$ for Tunable Electronic and Photocatalytic Properties. *Sci. Rep.* **2017**, *7*, 17088.

(10) Ren, X.; Ma, Q.; Fan, H.; Pang, L.; Zhang, Y.; Yao, Y.; Ren, X.; Liu, S. F. A Se-doped MoS_2 nanosheet for improved hydrogen evolution reaction. *Chem. Commun.* **2015**, *51*, 15997−16000.

(11) Xu, C.; Peng, S.; Tan, C.; Ang, H.; Tan, H.; Zhang, H.; Yan, Q. Ultrathin S-doped $MoSe_2$ nanosheets for efficient hydrogen evolution. *J. Mater. Chem. A* **2014**, *2*, 5597−5601.

(12) Ma, X.; Li, J.; An, C.; Feng, J.; Chi, Y.; Liu, J.; Zhang, J.; Sun, Y. Ultrathin Co(Ni)-doped MoS_2 nanosheets as catalytic promoters enabling efficient solar hydrogen production. *Nano Res.* **2016**, *9*, 2284−2293.

(13) Wang, X.; Hong, M.; Zhang, F.; Zhuang, Z.; Yu, Y. Recyclable Nanoscale Zero Valent Iron Doped g-C_3N_4/MoS_2 for Efficient Photocatalysis of RhB and Cr(VI) Driven by Visible Light. *ACS Sustainable Chem. Eng.* **2016**, *4*, 4055−4063.

(14) Huang, H.; Feng, X.; Du, C.; Song, W. High-quality phosphorus-doped MoS_2 ultrathin nanosheets with amenable ORR catalytic activity. *Chem. Commun.* **2015**, *51*, 7903−7906.

(15) Kresse, G.; Hafner, J. Ab initiomolecular dynamics for liquid metals. *Phys. Rev. B: Condens. Matter Mater. Phys.* **1993**, *47*, 558−561.

(16) Kresse, G.; Hafner, J. Ab initiomolecular-dynamics simulation of the liquid-metal-amorphous-semiconductor transition in germanium. *Phys. Rev. B: Condens. Matter Mater. Phys.* **1994**, *49*, 14251−14269.

(17) Kresse, G.; Furthmüller, J. Efficiency of Ab-Initio Total Energy Calculations for Metals and Semiconductors Using a Plane-Wave Basis Set. *Comput. Mater. Sci.* **1996**, *6*, 15−50.

(18) Perdew, J. P.; Burke, K.; Ernzerhof, M. Generalized Gradient Approximation Made Simple. *Phys. Rev. Lett.* **1996**, *77*, 3865−3868.

(19) Hamann, D. R.; Schlüter, M.; Chiang, C. Norm-conserving Pseudopotentials. *Phys. Rev. Lett.* **1979**, *43*, 1494−1497.

(20) Zhao, Y.; Wang, W.; Li, C.; Xu, Y.; He, L. Tuning the magnetic properties of the monolayer $MoSe_2$ by nonmetal doping: First-principles study. *Solid State Commun.* **2018**, *281*, 6−11.

(21) Grimme, S.; Antony, J.; Ehrlich, S.; Krieg, H. A Consistent and Accurate Ab Initio Parametrization of Density Functional Dispersion Correction (DFT-D) for the 94 Elements H-Pu. *J. Chem. Phys.* **2010**, *132*, 154104.

(22) Grimme, S. Semiempirical GGA-type density functional constructed with a long-range dispersion correction. *J. Comput. Chem.* **2006**, *27*, 1787−1799.

(23) Ma, Q.; Odenthal, P. M.; Mann, J.; Le, D.; Wang, C. S.; Zhu, Y.; Chen, T.; Sun, D.; Yamaguchi, K.; Tran, T.; et al. Controlled Argon Beam-Induced Desulfurization of Monolayer Molybdenum Disulfide. *J. Phys.: Condens. Matter* **2013**, *25*, 252201.

(24) He, L.; Xiu, F.; Yu, X.; Teague, M.; Jiang, W.; Fan, Y.; Kou, X.; Lang, M.; Wang, Y.; Huang, G.; et al. Surface-Dominated Conduction in a 6 nm thick Bi_2Se_3 Thin Film. *Nano Lett.* **2012**, *12*, 1486−1490.

(25) Kou, X.; Lang, M.; Fan, Y.; Jiang, Y.; Nie, T.; Zhang, J.; Jiang, W.; Wang, Y.; Yao, Y.; He, L.; et al. Interplay between Different Magnetisms in Cr-Doped Topological Insulators. *ACS Nano* **2013**, *7*, 9205−9212.

(26) Sun, Y.; Wang, D.; Shuai, Z. Indirect-to-Direct Band Gap Crossover in Few-Layer Transition Metal Dichalcogenides: A Theoretical Prediction. *J. Phys. Chem. C* **2016**, *120*, 21866−21870.

(27) Böker, T.; Severin, R.; Müller, A.; Janowitz, C.; Manzke, R. Band Structure of MoS_2, $MoSe_2$, and α-$MoTe_2$: Angle-Resolved

Photoelectron Spectroscopy and Ab Initio Calculations. *Phys. Rev. B: Condens. Matter Mater. Phys.* **2001**, *64*, 235305.
(28) Williamson, I.; Li, S.; Correa Hernandez, A.; Lawson, M.; Chen, Y.; Li, L. Structural, electrical, phonon, and optical properties of Ti- and V-doped two-dimensional MoS_2. *Chem. Phys. Lett.* **2017**, *674*, 157−163.
(29) Robertson, A. W.; Lin, Y.-C.; Wang, S.; Sawada, H.; Allen, C. S.; Chen, Q.; Lee, S.; Lee, G.-D.; Lee, J.; Han, S.; et al. Atomic Structure and Spectroscopy of Single Metal (Cr, V) Substitutional Dopants in Monolayer MoS2. *ACS Nano* **2016**, *10*, 10227−10236.
(30) Zhao, Y. F.; Li, C.; Hu, J. Y.; Gong, Y. Y.; Niu, L. Y.; Liu, X. J. Ta and N modulated electronic, optical and photocatalytic properties of TiO_2. *Phys. Lett. A* **2016**, *380*, 910−916.
(31) Zhao, Y.; Wang, W.; Li, C.; He, L. Electronic and photocatalytic properties of N/F co-doped anatase TiO_2. *RSC Adv.* **2017**, *7*, 55282−55287.
(32) Tian, H.; Liu, M.; Zheng, W. Constructing 2D graphitic carbon nitride nanosheets/layered MoS_2/graphene ternary nanojunction with enhanced photocatalytic activity. *Appl. Catal., B* **2018**, *225*, 468−476.
(33) West, A. R. *Basic Solid State Chemistry*; JohnWiley: Chichester, U.K., 1999.
(34) Wang, T. H.; Zhu, Y. F.; Jiang, Q. Bandgap Opening of Bilayer Graphene by Dual Doping from Organic Molecule and Substrate. *J. Phys. Chem. C* **2013**, *117*, 12873−12881.
(35) Yu, J.; Zhou, P.; Li, Q. New insight into the enhanced visible-light photocatalytic activities of B-, C- and B/C-doped anatase TiO_2 by first-principles. *Phys. Chem. Chem. Phys.* **2013**, *15*, 12040.
(36) Zhou, P.; Yu, J.; Wang, Y. The new understanding on photocatalytic mechanism of visible-light response NS codoped anatase TiO_2 by first-principles. *Appl. Catal., B* **2013**, *142−143*, 45−53.
(37) Wang, S.; Bai, L. N.; Sun, H. M.; Jiang, Q.; Lian, J. S. Structure and photocatalytic property of Mo-doped TiO_2 nanoparticles. *Powder Technol.* **2013**, *244*, 9−15.
(38) Toroker, M. C.; Kanan, D. K.; Alidoust, N.; Isseroff, L. Y.; Liao, P.; Carter, E. A. First Principles Scheme to Evaluate Band Edge Positions in Potential Transition Metal Oxide Photocatalysts and Photoelectrodes. *Phys. Chem. Chem. Phys.* **2011**, *13*, 16644−16654.

DOI: 10.1021/acs.jpcc.8b09361
J. Phys. Chem. C 2018, 122, 26570−26575